DYNAMIC MECHANICAL ANALYSIS IN THE ANALYSIS OF POLYMERS AND RUBBERS

1. Introduction and History of DMA

Dynamic mechanical analysis (DMA) is the technique of applying a stress or strain to a sample and analyzing the response to obtain phase angle and deformation data. These data allow the calculation of the damping or tan delta (δ) as well as complex modulus and viscosity data. Two approaches are used: (a) forced frequency, where the signal is applied at a set frequency and (b) free resonance, where the material is perturbed and allowed to exhibit free resonance decay. Most DMAs are the former type, whereas the torsional braid analyzer is the latter. In both approaches, the technique is very sensitive to the motions of the polymer chains and it is a powerful tool for measuring transitions in polymers. More specialized techniques such as the use of ultrasonics, laser pulses, and so on do exist in specialized markets (1). It is estimated to be 100 times more sensitive to the glass transition than differential scanning calorimetry (DSC), and it resolves other more localized transitions such as side chain movements that are not detected in the DSC. In addition, the technique allows the rapid scanning of a material's modulus and viscosity as a function of temperature, strain, or frequency. DMA may also be referred to as dynamic mechanical thermal analysis (DMTA), dynamic mechanical spectroscopy, or dynamic thermomechanical analysis.

DMA is a very important tool in the modern polymer laboratory. Despite that, only a few books have concentrated on the technique (2). The first attempt to do oscillatory experiments to measure the elasticity of a material was by Poynting (3) in 1909. Other early work gave methods to apply oscillatory deformations by various means to study metals (4), and many early experimental techniques were reviewed by te Nijenhuis (5) in 1978. Miller's book on polymer properties (6) referred to dynamic measurements in this early discussion of molecular structure and stiffness. Early commercial instruments included the Weissenberg rheogoniometer (~1950) and the Rheovibron (~1958). The Weissenberg rheogoniometer, which dominated cone-and-plate measurements for over 20 years following 1955, was the commercial version of the first instrument to measure normal forces (7). By the time, Ferry wrote the *Viscoelastic Properties of Polymers* (8) in 1961**,** dynamic measurements were an integral part of polymer science and he gives the best development of the theory available. In 1967, McCrum and co-workers (9) collected the current information on DMA and DEA (dielectric analysis) into his landmark textbook. The technique remained fairly specialized until the late

DOI: 10.1002/0471440264.pst102.pub2

sixties when commercial instruments became more user-friendly. About 1966, Gillham developed the TBA (10) and started the modern period of DMA. In 1971, Starita and Macosko (11) built a DMA that measured normal forces and from this came the Rheometrics Corporation. In 1976, Bohlin also developed a commercial DMA and started Bohlin Rheologia. Both instruments used torsional geometry. The early instruments were, regardless of manufacturer, difficult to use, slow, and limited in their ability to process data. In the late seventies, Murayani (12) and Read and Brown (13) wrote books on the uses of DMA for material characterization. Several thermal and rheological instrument companies introduced DMA's in the same time period, and currently most thermal and rheological vendors offer some type of DMA. Polymer Labs offered a dynamic mechanical thermal analyzer (DMTA using an axial geometry in the early 1980s. This was soon followed by an instrument from Du Pont. Perkin-Elmer developed a controlled stress analyzer based on their thermomechanical analyzer (TMA) technology, which was designed for increased low-end sensitivity. Triton Technologies, acquired by Mettler Toledo in 2010, developed a very easy to use design that formalized both immersion and humidity methods. On the high force end of applications, Mettler Toledo also makes an instrument capable of 40 N loads and both Gabo and MetaVib work exclusively in high load instruments. Small vendors include Hitachi, Bosch, and others. The competition between vendors has led to easier to use, faster, and less expensive instruments. The revolution in computer technology, which has so affected the laboratory, changed the latter, and DMA of all types became more user-friendly as computers and software evolved. This movement to easier to use instruments has led to more use in quality control and the development of ASTM standards (14).

2. Theory and Operating Principles

2.1. Forced Frequency Analyzers. If a constant load applied to a sample begins to oscillate sinusoidally (Fig. 1), the sample will deform sinusoidally. This will be reproducible if the material is deformed within its linear viscoelastic region. For any one point on the curve, the stress applied is described in equation (1)

$$\sigma = \sigma_0 \sin \omega t \tag{1}$$

where σ is the stress at time t, σ_0 is the maximum stress, ω is the frequency of oscillation, and t is the time. The resulting strain wave shape will depend on how much viscous behavior the sample has as well as how much elastic behavior. In addition, the rate of stress can be determined by taking the derivative of the above equation in terms of time:

$$\mathrm{d}\sigma/\mathrm{d}t = \omega\sigma_o \cos \omega t \tag{2}$$

The two extremes of the material's behavior, elastic and viscous, provide the limiting extremes that will sum to give the strain wave. The behavior can be understood by evaluating each of the two extremes. The material at the spring-like or

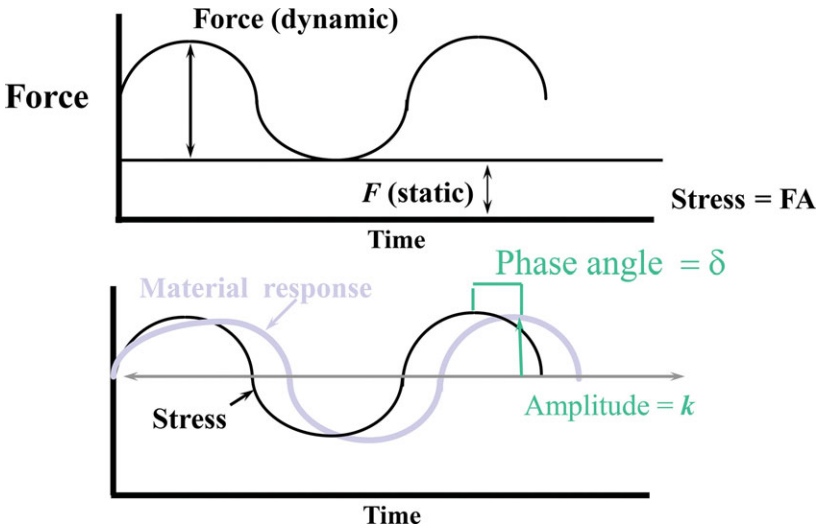

Fig. 1. Oscillating stress applied to a sample.

Hookean limit will respond elastically with the oscillating stress. The strain at any time can be written as

$$\varepsilon(t) = Es_o \sin(\omega t) \tag{3}$$

where $\varepsilon(t)$ is the strain at anytime t, E is the modulus, σ_0 is the maximum stress at the peak of the sine wave, and ω is the frequency. Since in the linear region σ and ε are linearly related by E, the relationship is

$$\varepsilon(t) = \varepsilon_o \sin(\omega t) \tag{4}$$

where ε_0 is the strain at the maximum stress. This curve shown in Figure 2**a** has no phase lag (or no time difference from the stress curve) and is called the in-phase portion of the curve.

The viscous limit was expressed as the stress being proportional to the strain rate, which is the first derivative of the strain. This is best modeled by a dashpot and for that element, the term for the viscous response in terms of strain rate is described as

$$\varepsilon(t) = \eta \mathrm{d}\sigma_0/\mathrm{d}t = \eta\omega\sigma_o \cos(\omega t) \tag{5}$$

or

$$\varepsilon(t) = \eta\omega\sigma_o \sin(\omega t + \pi/2) \tag{6}$$

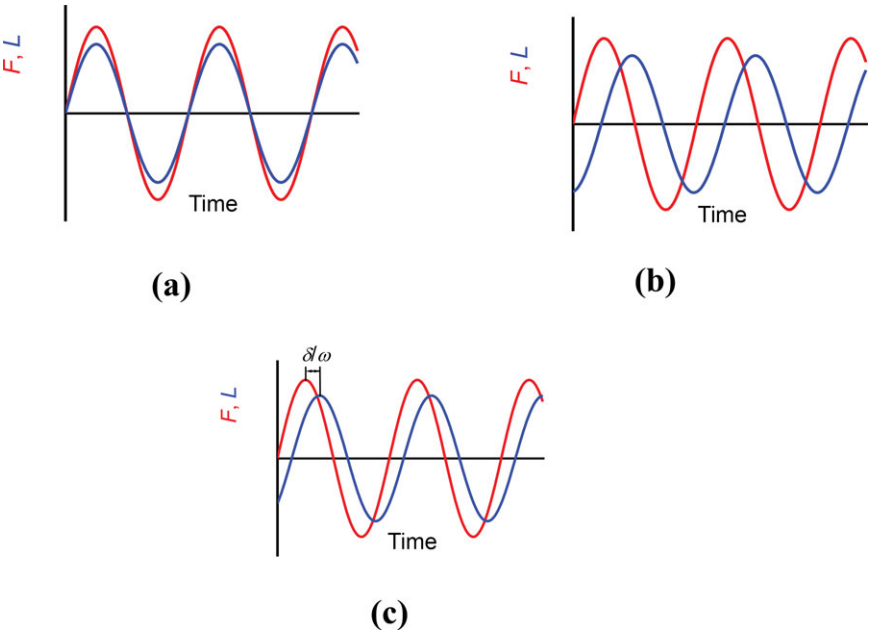

Fig. 2. Material responses in DMA.

where the terms are as above and η is the viscosity. Substituting terms as above makes the equation

$$\varepsilon(t) = \omega\sigma_o \cos(\omega t) = \omega\sigma_o \sin(\omega t + \pi/2) \tag{7}$$

This curve is shown in Figure 2**b**. Now, take the behavior of the material that lies between these two limits. That curve is shown in Figure 2**c** and is intermediate between the above cases. The difference between the applied stress and the resultant strain is an angle, δ, and this must be added to equations. So the elastic response at anytime can now be written as

$$\varepsilon(t) = \varepsilon_o \sin(\omega t + \delta) \tag{8}$$

Using trigonometry, this can be rewritten as

$$\varepsilon(t) = \varepsilon_o[\sin(\omega t)\cos\delta + \cos(\omega t)\sin\delta] \tag{9}$$

This equation, corresponding to the curve in Figure 2**c**, can be separated into the in-phase and out-of-phase strains that corresponds to curves like those in Figures 2**a** and 2**b,** respectively. These sum to the curve in Figure 2**c** and are

$$\varepsilon' = \varepsilon_o \sin(\delta) \tag{10}$$

$$\varepsilon'' = \varepsilon_o \cos(\delta) \tag{11}$$

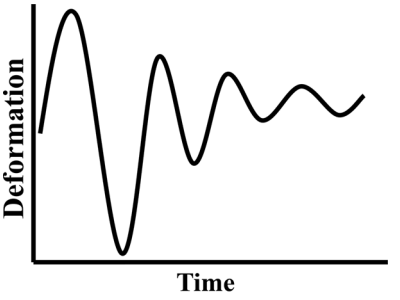

(a)

Fig. 3. Decay curve.

and the vector sum of these two components gives the overall or complex strain on the sample:

$$\varepsilon^* = \varepsilon' + i\varepsilon'' \tag{12}$$

2.2. Free Resonance Analyzers. If a suspended sample can swing freely, it will oscillate like a harp or guitar string until the oscillations gradually come to a stop. The naturally occurring damping of the material controls the decay of the oscillations. This produces a wave, shown in Figure 3, which is a series of sine waves decreasing in amplitude and frequency. Several methods exist to analyze these waves and are covered in the review by Gillham (15). These methods have also been successfully applied to the recovery portion of a creep-recovery curve where the sample goes into free resonance on removal of the creep force (16).

From the decay curve, the period, T, and the logarithmic decrement, Λ, can be calculated. Several methods exist for both manual and digital processing (15, 17). Fuller details of the following may be found in McCrum and colleagues (17) and Gillham (15). Basically the decay of the amplitude is evaluated over as many swings as possible to reduce error:

$$\Lambda = 1/j \ln \left(A_n/A_{(n+j)}\right) \tag{13}$$

where j is the number of swings and A_n is the amplitude of the nth swing. For one swing, where $j = 1$, the equation becomes

$$\Lambda = \ln \left(A_n/A_{(n+j)}\right) \tag{14}$$

if for a low value of Λ where A_n/A_{n+1} is approximately 1, the equation can be rewritten as

$$\Lambda \approx \frac{1}{2} \left(\left({A_n}^2 - {A_{n+1}}^2\right)/{A_n}^2\right) \tag{15}$$

from this, since the square of the amplitude is proportional to the stored energy, $\Delta W/W_{st}$, and the stored energy can be expressed as $2\pi \tan \delta$, the equation becomes

$$\Lambda \approx \tfrac{1}{2}(\Delta W/W_{st}) = \pi \tan \delta \tag{16}$$

which gives us the phase angle, δ. The time of the oscillations, the period, T, can be found using the following equation:

$$T = 2\pi\sqrt{\frac{M}{\Gamma_1}}\sqrt{\frac{1+\Lambda^2}{4\pi^2}} \tag{17}$$

where Γ_1 is the torque for one cycle and M is the moment of inertia around the central axis. Alternatively, T can be calculated directly from the plotted decay curve as

$$T = (2/n)(t_n - t_0) \tag{18}$$

where n is the number of cycles and t is time. From this, the shear modulus, G, can be calculated, which for a rod of length, L, and radius, r, is

$$G = \left(\frac{4\pi^2 ML}{NT^2}\right)\left(1 + \frac{\Lambda^2}{4\pi^2}\right) - \left(\frac{mgr}{12N}\right) \tag{19}$$

where m is the mass of the sample, g the gravitational constant and N is a geometric factor. In the same system, the storage modulus, G', can be calculated as

$$G' = (1/T^2)(8\pi ML/r^4) \tag{20}$$

Having the storage modulus and the tangent of the phase angle, the remaining dynamic properties can be calculated.

Free resonance analyzers normally are limited to rod or rectangular samples or materials that can be impregnated onto a braid. This last approach is how the curing studies on epoxy and other resin systems were done in torsion and gives these instruments the name of torsional braid analyzers (TBA).

3. Instrumentation

One of the biggest choices made in selecting a DMA is to decide whether to chose stress (force) or strain (displacement) control for applying the deforming load to the sample (Figs. 4**a** and 4**b**). Strain-controlled analyzers, whether for simple static testing or for DMA, move the probe a set distance and use a force balance transducer or load cell to measure the stress. These parts are typically located on different shafts. The simplest version of this is a screw-driven tester, where the sample is pulled one turn. This requires very large motors so the available force

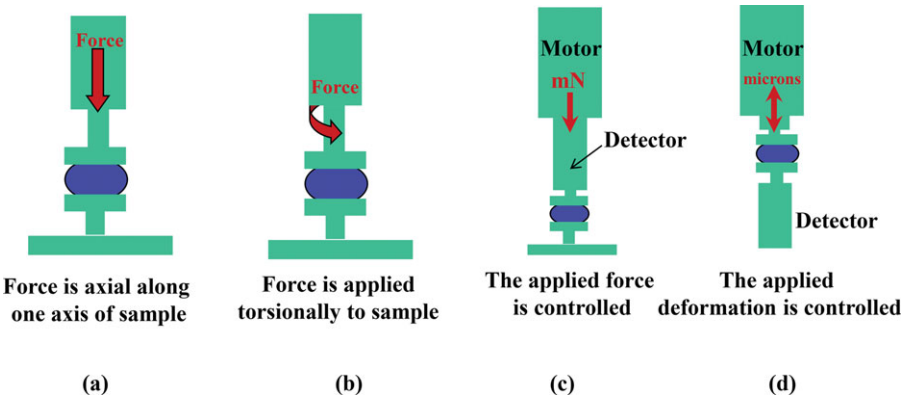

Fig. 4. Instrument types.

always exceeds what is needed. They normally have better short time response for low viscosity materials and can normally perform stress relaxation experiments easily. They also usually can measure normal forces if they are arranged in torsion. A major disadvantage is that their transducers may drift at long times or with low signals.

Stress-controlled analyzers are cheaper to make because there is only one shaft, but somewhat trickier to use. Many of the difficulties have been alleviated by software, and many strain-controlled analyzers on the market are really stress-controlled instruments with feedback loops making them act as if they were strain controlled. In stress control, a set force is applied to the sample. As temperature, time, or frequency varies, the applied force remains the same. This may or may not be the same stress: In extension, for example, the stretching and necking of a sample will change the applied stress seen during the run. However, this constant stress is a more natural situation in many cases and it may be more sensitive to material changes. Good low force control means they are less likely to destroy any structure in the sample. Long relaxation times or long creep studies are more easily preformed on these instruments. Their biggest disadvantage is that their short time responses are limited by inertia with low viscosity samples. Most stress-controlled rheometers today use a feedback loop to mimic strain control and some, like the Mettler Toledo DMA/SDTA861[e], will switch automatically from one mode to the other depending the samples behavior,

Since most DMA experiments are run at very low strains (~0.5% maximum) to stay well within a polymers linear region, it has been reported that the both analyzers give the same results. However, when one gets to the nonlinear region, the difference becomes significant as stress and strain are no longer linearly related. Stress control can be said to duplicate real-life conditions more accurately since most applications of polymers involve resisting a load. However, the choice is best made on the specific application.

DMA analyzers are normally built to apply the stress or strain in two ways (Figs. 4**c** and 4**d**). One can apply force in a twisting motion so one is testing the sample in torsion. This type of instrument is the dynamic analog of the constant shear spinning disk rheometers. While mainly used for liquids and melts, solid

samples may also tested by twisting a bar of the material. Torsional analyzers normally also permit continuous shear and normal force measurements. Most of these analyzers can also do creep-recovery, stress-relaxation, and stress–strain experiments.

Axial analyzers are normally designed for solid and semisolid materials and apply a linear force to the sample. These analyzers are usually associated with flexure, tensile, and compression testing, but they can be adapted to do shear and liquid specimens by proper choice of fixtures. Sometimes the instrument's design makes this inadvisable, however (eg, working with a very fluid material in a system where the motor is underneath the sample has the potential for damage to the instrument if the sample spills into the motor). These analyzers can normally test higher modulus materials than torsional analyzers and can run TMA studies in addition to creep-recovery, stress-relaxation, and stress–strain experiments.

Despite the traditional selection of torsional instruments for melts and liquids and axial instruments for solids, there is really considerable overlap between the types of instruments. With the proper choice of sample geometry and good fixtures, both types can handle similar samples, as shown by the use of both types to study the curing of neat resins. Normally axial analyzers can not handle fluid samples below about 2.5 Pa s, and torsional instruments will top out with the harder samples (the exact modulus depending on the size of the motor and/or load cell.)

4. Applications

4.1. Thermoplastic Solids and Cured Thermosets. The thermal transitions in polymers can be described in terms of either free volume changes (18) or relaxation times (19). While the latter tends to be preferred by engineers and rheologists in contrast to chemist and polymer physicists who lean toward the former, both descriptions are equivalent. Changes in free volume, v^f, can be monitored as a volumetric change in the polymer, by the absorption or release of heat associated with that change, the loss of stiffness, increased flow, or by the a change in relaxation time.

The free volume of a polymer, v^f, is known to be related to viscoelasticity (20), aging (21), penetration by solvents (22), and impact properties (23). Defined as the space a molecule has for internal movement, it is schematically shown in Figure 5**a**. A simple approach to looking at free volume is the crankshaft mechanism (24), where the molecule is imagined as a series of jointed segments. From this model, it is possible to simply describe the various transitions seen a polymer. Other models exist that allow for more precision in describing behavior; the best seems to be the Doi–Edwards model (25). Aklonis and Knight (26) give a good summary of the available models, as does Rohn (27).

The crankshaft model treats the molecule as a collection of mobile segments that have some degree of free movement. This is a very simplistic approach, yet very useful for explaining behavior. As the free volume of the chain segment increases, its ability to move in various directions also increases (Fig. 5**b**). This increased mobility in either side chains or small groups of adjacent backbone atoms results in a greater compliance (lower modulus) of the molecule. These

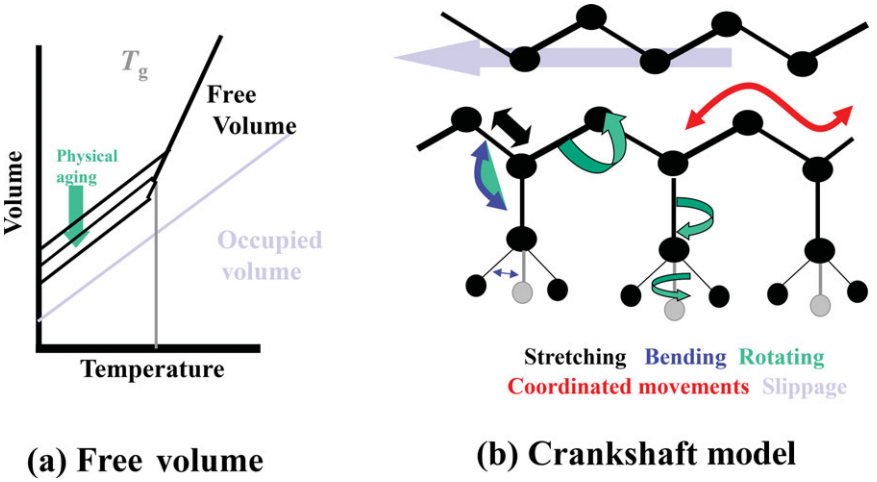

Fig. 5. Free volume and molecular motions in polymers.

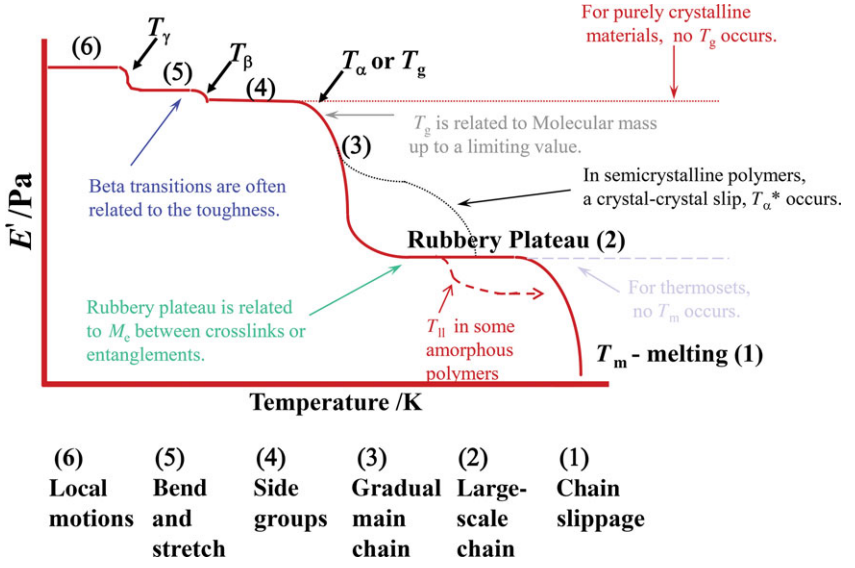

Fig. 6. Idealized DMA scan.

movements have been studied and Heijboer (28) classified β and γ transitions by their type of motions. The specific temperature and frequency of this softening help drive the end use of the material.

Moving from very low temperature, where the molecule is tightly compressed, to higher temperatures the first changes are the solid-state transitions. This process is shown in Figure 6. As the material warms and expands, the free volume increases so that localized bond movements (bending and stretching) and side chain movements can occur. This is the gamma transition, T_γ, which may also involve associations with water (29). As the temperature and the free volume

continue to increase, the whole side chains and localized groups of four to eight backbone atoms begin to have enough space to move and the material starts to develop some toughness (30). This transition, called the beta transition T_β, is not as clearly defined as described here (Fig. 6). Often it is the T_g of a secondary component in a blend or of a specific block in a block copolymer. However, a correlation with toughness is seen empirically (31).

As heating continues, the T_g or glass transition appears when the chains in the amorphous regions begin to coordinate large-scale motions (Fig. 6). One classical description of this region is that the amorphous regions have begun to melt. Since the T_g only occurs in amorphous material, in a 100% crystalline material there would not be a T_g. Continued heating drives the material through the T_α* and T_{ll} (Fig. 6**d**). The former occurs in crystalline or semicrystalline polymer and is a slippage of the crystallites past each other. The latter is a movement of coordinated segments in the amorphous phase that relates to reduced viscosity. These two transitions are not universally accepted. Finally, the melt is reached (Fig. 6**e**) where large-scale chain slippage occurs and the material flows. This is the melting temperature, T_m. For a cured thermoset, nothing happens after the T_g until the sample begins to burn and degrade because the cross-links prevent the chains from slipping past each other.

This quick overview provides an idea of how an idealized polymer responds. Now a more detailed description of these transitions can be provided with some examples of their applications. The best general collection of this information is still McCrum's 1967 text (24).

4.1.1. Sub-T_g Transitions. The area of sub-T_g or higher order transitions has been heavily studied (32) as these transitions have been associated with mechanical properties. These transitions can sometimes be seen by DSC and TMA, but they are normally too weak or too broad for determination by these methods. DMA, DEA, and similar techniques are usually required (33). Some authors have also called these types of transitions (34) second-order transitions to differentiate them from the primary transitions of T_m and T_g, which involve large sections of the main chains. Boyer reviewed the T_β in 1968 (35) and pointed out that while a correlation often exists, the T_β is not always an indicator of toughness. Bershtein and Egorov (36) have reported that this transition can be considered the "activation barrier" for solid-phase reactions, deformation, flow or creep, acoustic damping, physical aging changes, and gas diffusion into polymers as the activation energies for the transition, and these processes are usually similar. The strength of these transitions is related to how strongly a polymer responses to those processes. These sub-T_g transitions are associated with the materials properties in the glassy state. In paints, for example, peel strength (adhesion) can be estimated from the strength and frequency dependence of the subambient beta transition (37). Nylon 6,6 shows a decreasing toughness, measured as impact resistance, with declining area under the T_β peak in the tan δ curve. Figure 7 shows the relative differences in the T_β compared to the T_g for a high impact and low impact nylon. It has been shown, particularly in cured thermosets, that increased freedom of movement in side chains increases the strength of the transition. Cheng and co-workers (38) report in rigid rod polyimides that the beta transition is caused by the noncoordinated movement of the diamine groups al-

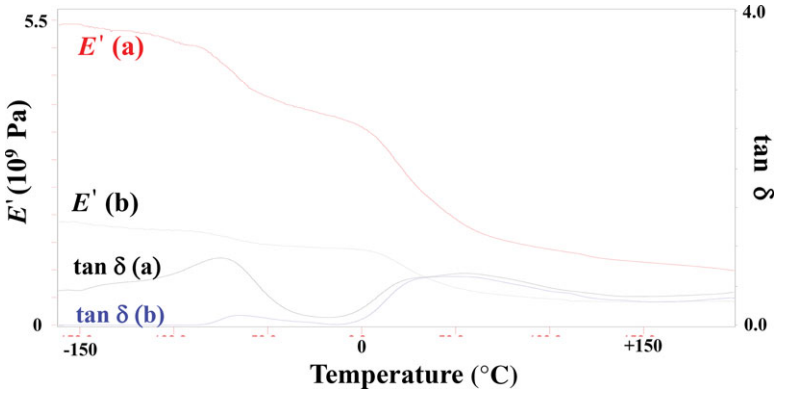

Fig. 7. Beta transitions and toughness.

though the link to physical properties was not investigated. Johari and their associates have reported in both mechanical (39) and dielectric studies (40) that both the β and γ transitions in bisphenol-A based thermosets depend on the side chains and unreacted ends, and that both are affected by physical aging and postcure. Nelson (41) has reported that these transitions can be related to vibration damping. This is also true for acoustical damping (42). In both of this cases, the strength of the beta transition is taken as a measurement of how effectively a polymer will absorb vibrations. There is some frequency dependence involved in this, which will be discussed later in Section 5.7.

Boyer (43) and Heijober (28) showed that this information needs to be considered with care as not all beta transitions correlate with toughness or other properties. This can be due to misidentification of the transition, or that the transition does sufficiently disperse energy. A working rule of thumb (44) is that the beta transition must be related to either localized movement in the main chain or very large side chain movement to sufficiently absorb enough energy. The relationship of large side chain movement and toughness has been extensively studied in polycarbonate by Yee (45) as well as in many other tough glassy polymers (46).

Less use is made of the T_γ transitions, and they are mainly studied to understand the movements occurring in polymers. Wendorff (47) reports that this transition in polyarylates is limited to inter- and intramolecular motions within the scale of a single repeat unit. Both McCrum and co-workers (24) and Boyd (48) similarly limited the T_γ and T_δ to very small motions either within the molecule or with bound water. The use of what is called 2D-IR, which couples at FTIR and a DMA to study these motions, is a topic of current interest (49).

4.1.2. The Glass Transition (T_g or T_α). As the free volume continues to increase with increasing temperature, the glass transition, T_g, occurs where large segments of the chain start moving. This transition is also called the alpha transition, T_α. The T_g is very dependent on the degree of polymerization up to a value known as the critical T_g or the critical molecular weight. Above this value, the T_g typically becomes independent of molecular weight (50). The T_g represents a

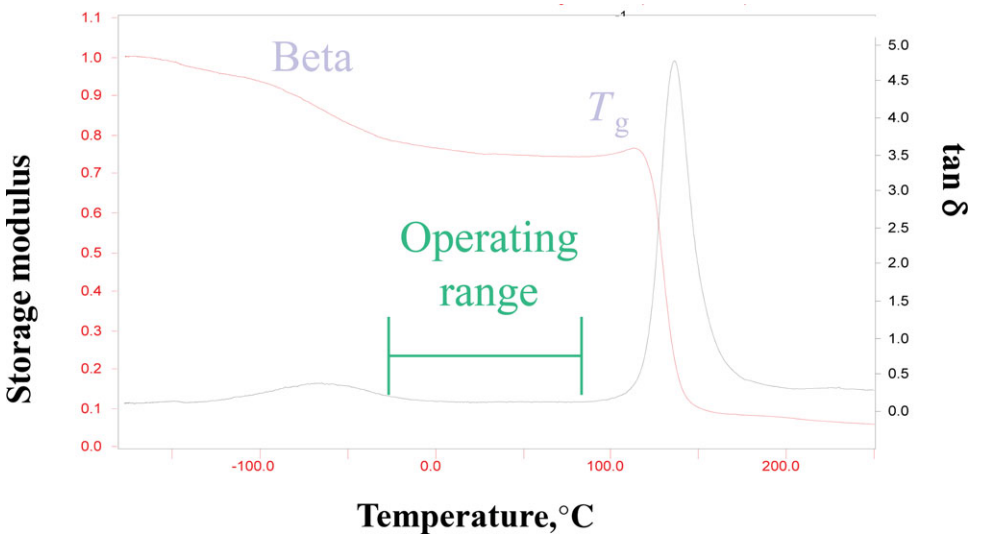

Fig. 8. Operating range by DMA.

major transition for many polymers, as physical properties changes drastically as the material goes from a hard glassy to a rubbery state. It defines one end of the temperature range over which the polymer can be used, often called the operating range of the polymer, and an example of this range is shown in Figure 8. For where strength and stiffness are needed, it is normally the upper limit for use. In rubbers and some semicrystalline materials such as polyethylene and polypropylene, it is the lower operating temperature. Changes in the temperature of the T_g are commonly used to monitor changes in the polymer such as plasticizing by environmental solvents and increased cross-linking from thermal or UV aging.

The T_g of cured materials or thin coatings is often difficult to measure by other methods, and more often than not the initial cost justification for a DMA is measuring a hard to find T_g. While estimates of the relative sensitivity of DMA to DSC or DTA vary, it appears that DMA is 10–100 times more sensitive to the changes occurring at the T_g. The T_g in highly cross-linked materials can easily be seen long after the T_g has become too flat and diffuse to be seen in the DSC (Fig. 9). A highly cross-linked molding resin used for chip encapsulation was run by both methods, and the DMA is able to detect the transition after it is undetectable in the DSC. This is also a known problem with certain materials such as medical-grade urethanes and very highly crystalline polyethylenes.

The method of determining the T_g in the DMA can be a manner for disagreement as at least five ways that are in current use (Fig. 10a). It should be noted that DSC has multiple methods too (Fig. 10**b**). Depending on the industry standards or background of the operator, the peak or onset of the tan δ curve, the onset of the E' drop, or the onset or peak of the E'' curve may be used. The values obtained from these methods can differ up to 25°C from each other on the same run. In addition, a 10–20°C difference from the DSC is also seen in many materials. In practice, it is important to specify exactly how the T_g should be determined. For DMA, this means defining the heating rate, applied stresses (or strains), the

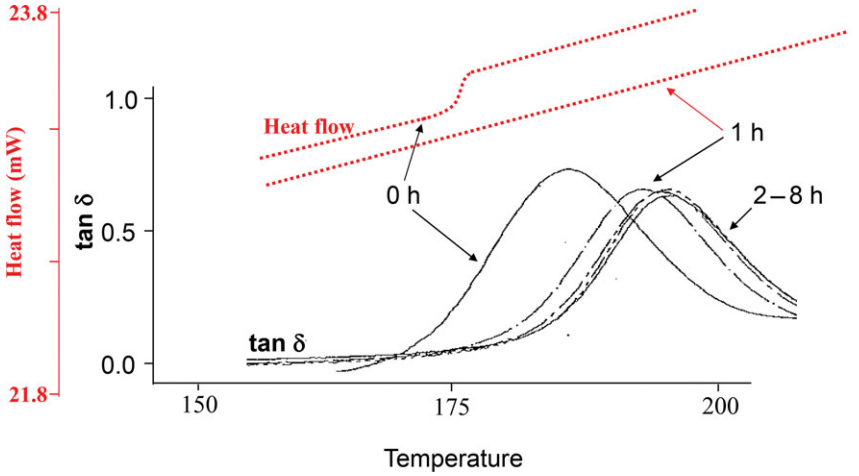

Fig. 9. Electronic encapsulation material by DMA and DSC.

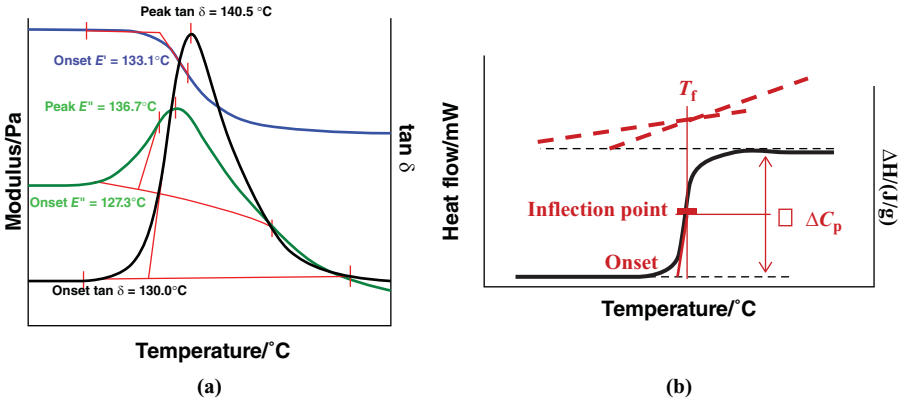

Fig. 10. T_g by DMA and DSC.

frequency used, and the method of determining the T_g. For example, the sample will be run at 10°C min^{-1} under 0.05% strain at 1 Hz in nitrogen purge (20 cc min^{-1}) and the T_g determined from peak of the tan δ curve.

It is not unusual to see a peak or hump on the storage modulus directly preceding the drop that corresponds to the T_g. This is shown in Figure 11. This is also seen in the DSC and DTA and corresponds to a rearrangement in the molecule to relieve stresses frozen in below the T_g by the processing method. These stresses are trapped in the material until enough mobility is obtained at the T_g to allow the chains to move to a lower energy state. Often a material will be annealed by heating it above the T_g and slowly cooling it to remove this effect. For similar reasons, some experimenters will run a material twice or use a heat—cool–heat cycle to eliminate processing effects.

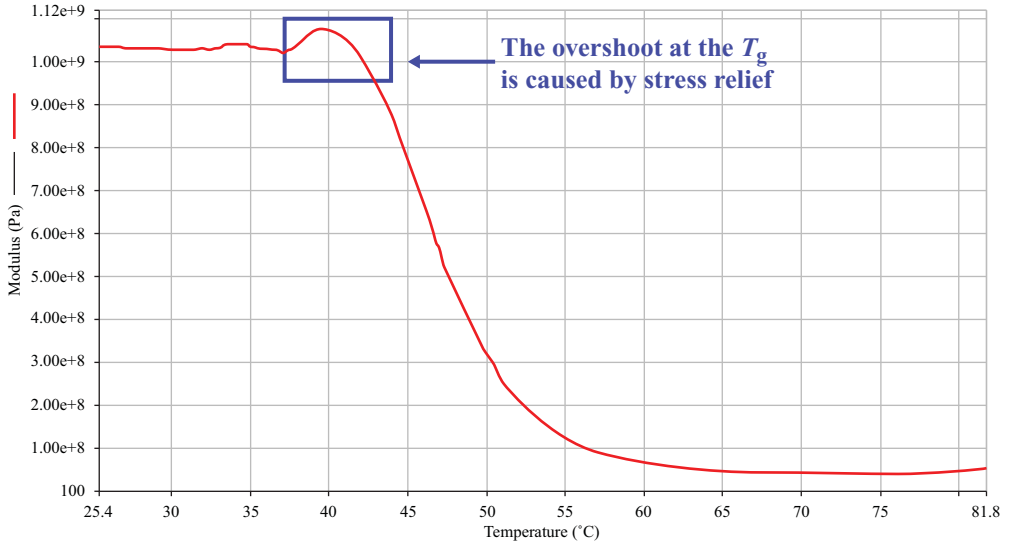

Fig. 11. Stress relief.

4.1.3. The Rubbery Plateau, T_α and T_{ll}.* The area above the T_g and below the melt is known as the rubbery plateau, and the length of it as well as its viscosity is dependent on the molecular weight between entanglements (M_e) (51) or cross-links. The molecular weight between entanglements is normally calculated during a stress-relaxation experiment, but similar behavior is observed in the DMA. The modulus in the plateau region is proportional to either the number of cross-links or the chain length between entanglements. This is often expressed in shear as

$$G' \cong (\rho RT)/M_e \tag{21}$$

where G′ is the shear storage modulus of the plateau region at a specific temperature, ρ is the polymer density, and M_e is the molecular weight between entanglements. In practice, the relative modulus of the plateau region shows the relative changes in M_e or the number of cross-links compared to a standard material.

The rubbery plateau is also related to the degree of crystallinity in a material, although DSC is a better method for characterizing crystallinity than DMA (52). Also as in the DSC, there is evidence of cold crystallization in the temperature range above the T_g (Fig. 12). That is one of several transitions that can be seen in the rubbery plateau region. This crystallization occurs when the polymer chains have been quenched (quickly cooled) into a highly disordered state. On heating above the T_g, these chains gain enough mobility to rearrange into crystallites, which causes sometimes a dramatic increase in modulus. DSC or one of its temperature-modulated (MT-DSC) variants, such as Mettler's ADSC or TOPEM or PerkinElmer's StepScan, or Water's TMDSC, for example, can be used to confirm this (53). The alpha star transition, T_α*, the liquid–liquid transition, T_{ll}, the heat set temperature, and the cold crystallization peak are

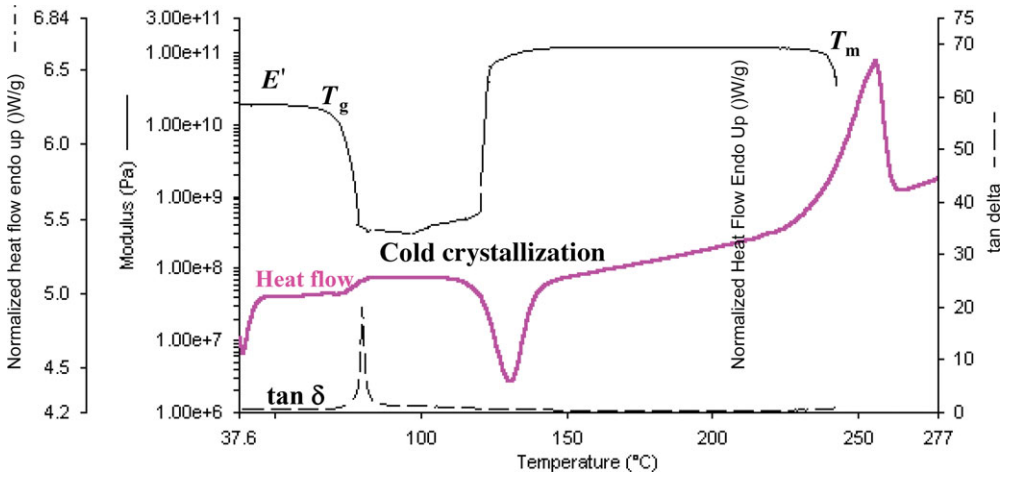

Fig. 12. Cold crystallization in PET.

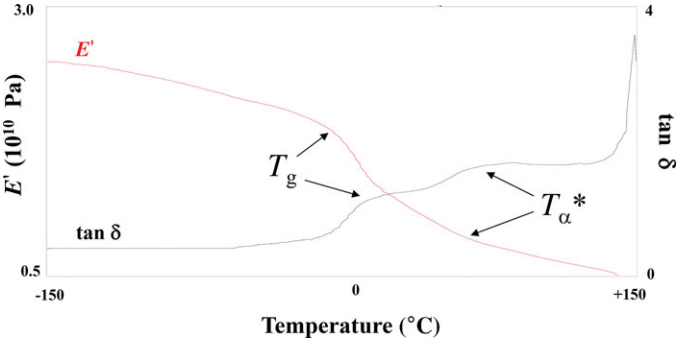

Fig. 13. Crystal-crystal slip.

all transitions that can appear on the rubbery plateau. In some crystalline and semicrystalline polymer, a transition is seen here called the T_α* (54). Figure 13 shows this in a sample of polypropylene. The alpha star transition is associated with the slippage between crystallites and helps extend the operating range of a material above the T_g. This transition is very susceptible to processing-induced changes and can be enlarged on decreased by the applied heat history, processing conditions, and physical aging (55). The T_α* has been used by fiber manufacturers to optimize properties in their materials.

In amorphous polymers, the T_{ll} transition is seen instead, which is a liquid–liquid transition associated with increased chain mobility and segment–segment associations (56). This order is lost when the T_{ll} is exceeded and regained on cooling from the melt. Boyer (57) reports that, like the T_g, the appearance of the T_{ll} is affected by the heat history. The T_{ll} is also dependent on the number average molecular weight, M_n, but not on the weight average molecular weight, M_w. Bershtein and co-workers (58) suggest that this may be considered as quasi-melting on heating or the formation of stable associates of segments

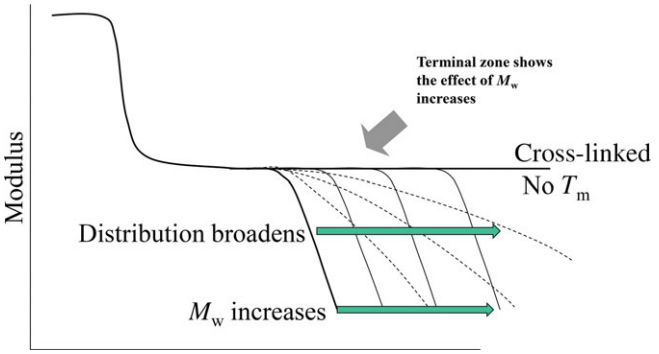

Fig. 14. Effect of M_W on flow.

on cooling. While this transition is reversible, it is not always easy to see, and Boyer (59) spent many years trying to prove it was real. Not everyone accepts the existence of this transition. This transition may be similar to some of the data from temperature-modulated DSC experiments showing a recrystallization at the start of the melt (60). In both cases, some subtle changes in structure are sometimes detected at the start of melting. Following this transition, a material enters the terminal or melting region.

Depending on its strength, the heat set temperature can also be seen in the DMA. While it is normally seen in either a TMA or a Constant Gauge Length (CGL) experiment, it will sometimes appear as either a sharp drop in storage modulus (E') or an abrupt change in probe position. Heat set is the temperature at which some strain or distortion is induced into polymeric fibers to change its properties, such as to prevent a nylon rug from feeling like fishing line. Since heating above this temperature will erase the texture, and polyesters must be heated above the T_g to dye them, it is of critical importance to the fabric industry. Many final properties of polymeric products depend on changes induced in processing (61).

4.1.4. The Terminal Region. On continued heating, the melting point, T_m, is reached. The melting point is where the free volume has increased so the chains can slide past each other and the material flows. This is also called the terminal region. In the molten state, this ability to flow is dependent on the molecular weight of the polymer (Fig. 14). The melt of a polymer material will often show changes in temperature of melting, width of the melting peak, and enthalpy as the material changes (62), resulting from changes in the polymer molecular weight and crystallinity.

Degradation, polymer structure, and environmental effects all influence what changes occur. Polymers that degrade by cross-linking will look very different from those that exhibit chain scission. Very highly cross-linked polymers will not melt as they are unable to flow.

The study of polymer melts and especially their elasticity was one of the areas that drove the development of commercial DMAs. Although a decrease in the melt viscosity is seen with temperature increases, the DMA is most commonly

Table 1. ASTM Tests for the DMA

D3386	CTE of Electrical Insulating Materials by TMA
D4065	Determining DMA Properties Terminology[a]
D4092	Terminology for DMA Tests
D4440	Measurement of Polymer Melts
D4473	Cure of Thermosetting Resins
D5023	DMA in Three Point Bending Tests
D5024	DMA in Compression
D5026	DMA in Tension
D5279	DMA of Plastics in Torsion
D5418	DMA in Dual Cantilever
D7028	Glass Transition Temperature of Polymer Matrix Composites
D7750	Cure Behavior of Thermosetting Resins by DMA using an Encapsulated Specimen Rheometer
E 228	CTE by TMA with Silica Dilatometer
E 473	Terminology for Thermal Analysis
E-756	Measuring Vibration-Damping Properties of Materials
E 831	CTE of Solids by TMA
E 1363	Temperature Calibration for TMA
E 1545	T_g by TMA
E 1640	T_g by DMA
E 1824	T_g by TMA in Tension
E 1867	Temperature Calibration for DMA
E-1953	Standard Practice for Description of Thermal Analysis and Rheology Apparatus
E-2254	Standard Test Method for Storage Modulus Calibration of DMA
E-2425	Standard Test Method for Loss Modulus Conformance of DMA
F-3131	Specification for Epoxy/Cotton Raw Materials for the Use in Bearing Cages

[a]This standard qualifies a DMA as acceptable for all ASTM DMA Standards.

used to measure the frequency dependence of the molten polymer as well as its elasticity. The latter property, especially when expressed as the normal forces, is very important in polymer processing.

4.1.5. Frequency Dependencies in Transition Studies. The choice of a testing frequency or its effect on the resulting data must be addressed. A short discussion of how frequencies are chosen and how they affect the measurement of transitions is in order. Considering that higher frequencies induce more elastic-like behavior, there is some concern a material will act stiffer than it really is if the test frequency is chosen to be too high. Frequencies for testing are normally chosen by one of three methods. The most scientific method would be to use the frequency of the stress or strain that the material is exposed to in the real world. However, this is often outside of the range of the available instrumentation. In some cases, the test method or the industry standard sets a certain frequency and this frequency is used. Ideally a standard method like this is chosen so that the data collected on various commercial instruments can be shown to be compatible. Some of the ASTM methods for DMA are listed in Table 1. Many industries have their own standards so it is important to know whether the data are expected to match a Mil-spec, an ASTM standard, or a specific industrial test. Finally,

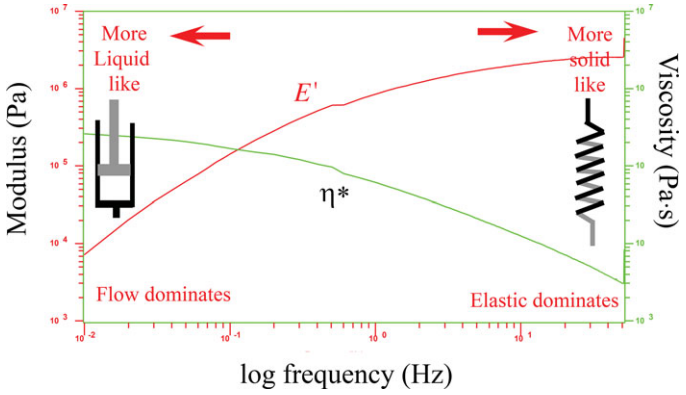

Fig. 15. General trends in frequency scans.

one can arbitrarily pick a frequency. This is done more often than not, so that 1 Hz and 10 rad s^{-1} are often used. As long as the data are run under the proper conditions, they can be compared to highlight material differences. This requires that frequency, stresses, and the thermal program be the same for all samples in the data set.

Lowering the frequency shifts the temperature of a transition to a lower temperature (Fig. 15). At one time, it was suggested that multiple frequencies could be used and the T_g should then be determined by extrapolation to 0 Hz. This was never really accepted as it represented a fairly large increase in testing time for a small improvement in accuracy. For most polymer systems, for very precise measurements, one uses a DSC. Different types of transitions also have different frequency dependencies; McCrum and co-workers (24) listed many of these. If one looks at the slope of the temperature dependence of transitions against frequency, one sees that in many cases the primary transitions such as T_m and T_g have a different dependence on frequency than the lower temperature transitions. In fact, the activation energies are different for α, β, and γ transitions because of the different motions required and the transitions can be sorted by this approach (2).

4.2. Polymer Melts and Solutions. A fluid or polymer melt responds to strain rate rather than to the amount of stress applied. The viscosity is one of the main reason why people run frequency scans. As the stress–strain curves and the creep recovery runs show, viscoelastic materials exhibit some degree of flow or unrecoverable deformation. The effect is strongest in melts and liquids where frequency versus viscosity plots are the major application of DMA.

Figure 16 shows a frequency scan on a viscoelastic material. In this example, the sample is a rubber above the T_g in three-point bending, but the trends and principles apply to both solids and melts. The storage modulus and complex viscosity are plotted on log scales against the log of frequency. In analyzing the frequency scans, trends in the data are more significant than specific peaks or transitions.

Starting with the viscosity curve, η^*, a fairly flat region appears at low frequency, called the zero shear plateau (63). This is where the polymer exhibits Newtonian behavior, and its viscosity is dependent on molecular weight, not the

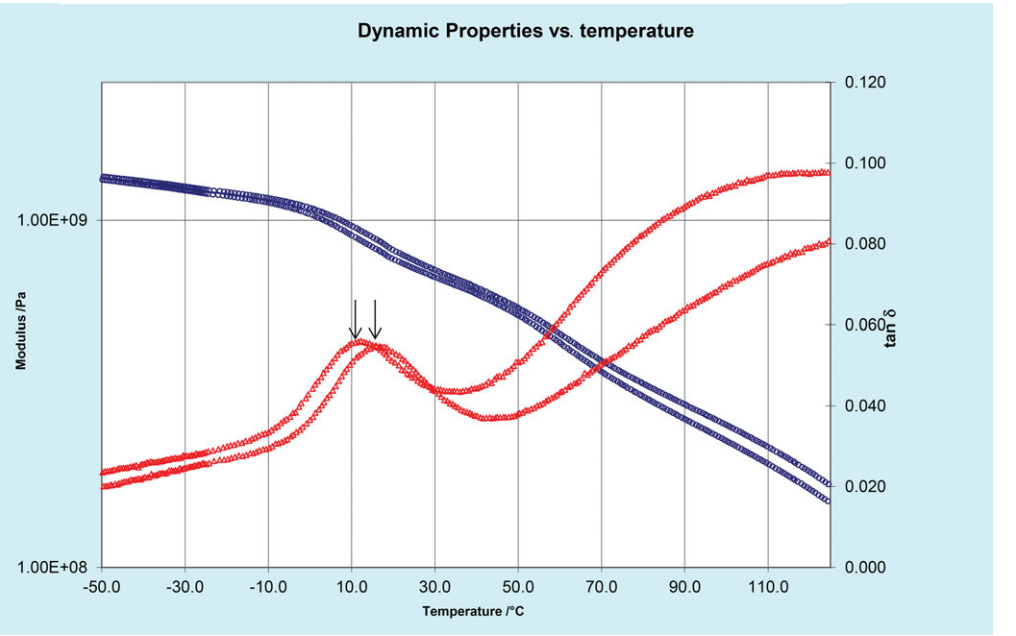

Fig. 16. Effect of frequency on transitions in filled polypropylene.

strain rate. The viscosity of this plateau has been shown to experimentally related to the molecular weight for Newtonian fluid:

$$\eta \propto cM_v^1 \tag{22}$$

for cases where the molecular weight, M_v, is less than the entanglement molecular weight, M_e and for cases where M_v is greater than M_e:

$$\eta \propto cM_v^{3.4} \tag{23}$$

where η_o is the viscosity of the initial Newtonian plateau, c is a material constant, and M_v the viscosity average molecular weight. This relationship can be written in general terms, replacing the exponential term with the Mark–Houwink constant, a. Equation 23 can be used as a method of approximating the molecular weight of a polymer. The value obtained is closest to the viscosity average molecular weight obtained by osmometry (64). In comparison with the weight average data obtained by gel permeation chromatography, the viscosity average molecular weight would be between the number average and weight average molecular weights, but closer to the latter (65). This was orginially developed for steady shear viscosity but applies to complex viscosity as well. The relationship between steady shear and complex viscosity is fairly well established. Cox and Merz (66) found that an empirical relationship exists between complex viscosity and steady

shear viscosity when the shear rates are the same. The Cox–Merz rule is stated:

$$\left|\eta(\omega)\right| = \eta(\dot{\gamma})\big|_{\dot{\gamma}=\omega} \tag{24}$$

where η is the constant shear viscosity, η^* is the complex viscosity, ω is the frequency of the dynamic test, and $d\gamma/dt$ is the shear rate of the constant shear test. This rule of thumb seems to hold for most materials to within about $\pm 10\%$. Another approach is the Gleissile's (67) mirror relationship that states the following:

$$\eta\dot{\gamma} = \eta^{+}(t)\big|_{t=1/\dot{\gamma}} \tag{25}$$

when $\eta^{+}(t)$ is the limiting value of the viscosity as the shear rate, $\dot{\gamma}$, approaches zero.

The low frequency range is where viscous or liquid-like behavior predominates. If a material is stressed over long enough times, some flow occurs. As time is the inverse of frequency, this means materials are expected to flow more at low frequency. As the frequency increases, the material will act in a more and more elastic fashion. Silly Putty, the children's toy, shows this clearly. At low frequency, Silly Putty flows like a liquid while at high frequency it bounces like a rubber ball.

This behavior is also similar to what happens with temperature changes. A polymer becomes softer and more fluid as it is heated, and it goes through transitions that increase the available space for molecular motions. Over long enough time periods, or small enough frequencies, similar changes occur. So one can move a polymer across a transition by changing the frequency. This relationship is also expressed as the idea of time–temperature equivalence (68). Often stated as low temperature is equivalent to short times or high frequency, it is a fundamental rule of thumb in understanding polymer behavior.

As the frequency is increased in a frequency scan, the Newtonian region is exceeded and a new relationship develops between the rate of strain, or the frequency, and the viscosity of the material. This region is often called the power law zone and can be modeled by

$$\eta^* \cong \eta(\dot{\gamma}) = c\dot{\gamma}^{n-1} \tag{26}$$

where η^* is the complex viscosity, $\dot{\gamma}$ is the shear rate, and the exponent term n is determined by the fitting of the data. The can also be written as

$$\sigma \cong \eta(\dot{\gamma}) = c\dot{\gamma}^{n} \tag{27}$$

where σ is the stress and η is the viscosity. The exponential relationship is why the viscosity versus frequency plot is traditionally plotted on a log scale. With modern curve-fitting programs, the use of log–log plots has declined and is a bit anachronistic. The power law region of polymers shows shear thickening or thinning behavior. This is also the region in which the E'–η^* or the E''–E'' crossover

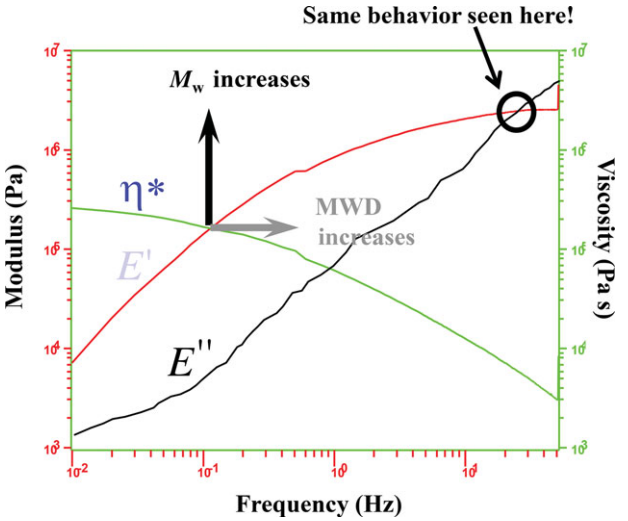

Fig. 17. M_w by crossover point.

point is found. As frequency increases and shear thinning occurs, the viscosity (η^*) decreases. At the same time, increasing the frequency increases the elasticity (E'). This is shown in Figure 17. The E'–η^* crossover point is used an indicator of the molecular weight and molecular weight distribution (69). Changes in its position are used as a quick method of detecting changes in the molecular weight and distribution of a material. After the power law region, another plateau is seen, the infinite shear plateau.

This second Newtonian region corresponds to where the shear rate is so high that the polymer no longer shows a response to increases in the shear rate. At the very high shear rates associated with this region, the polymer chains are no longer entangled. This region is seldom seen in DMA experiments and usually avoided in use because of the damage done to the chains. It can be reached in commercial extruders and causes degradation of the polymer, which causes the poorer properties associated with regrind.

As the curve in Figure 17 shows, the modulus also varies as a function of the frequency. A material exhibits more elastic-like behavior as the testing frequency increases and the storage modulus tends to slope upward toward higher frequency. The storage modulus' change with frequency depends on the transitions involved. Above the T_g, the storage modulus tends to be fairly flat with a slight increase with increasing frequency as it is on the rubbery plateau. The change in the region of a transition is greater. If one can generate a modulus scan over a wide enough frequency range (Fig. 18), the plot of storage modulus versus frequency appears like the reverse of a temperature scan. The same time–temperature equivalence discussed above also applies to modulus, as well as compliance, tan delta, and other properties.

The frequency scan is used for several purposes that will be discussed in this section. One very important use, that is very straightforward, is to survey the material's response over various shear rates. This is important because many

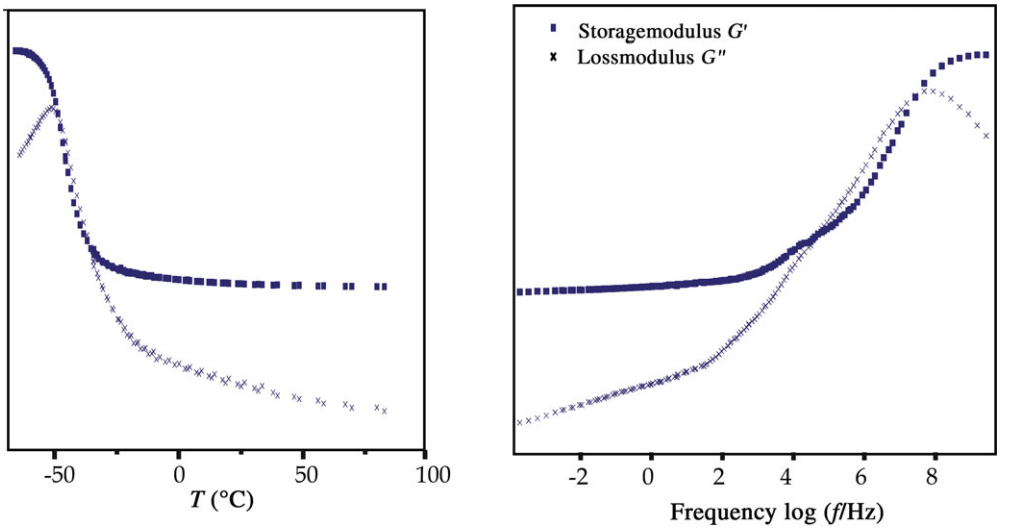

Fig. 18. Temperature and frequency scans.

materials are used under different conditions. For example, adhesives, whether tape, Band-Aids™, or hot melts, are normally applied under conditions of low frequency, and this property is referred to as tack. When they are removed, the removal often occurs under conditions of high frequency called peel. Different properties are required at these regimes, and to optimize one property may require chemical changes that harm the other. Similarly, changes in polymer structure can show these kinds of differences in the frequency scan. For example, branching affects different frequencies (25).

For example, in a tape adhesive, sufficient flow under pressure at low frequency is desired to fill the pores of the material to obtain a good mechanical bond. When the laminate is later subjected to peel, the material needs to be very elastic so it will not pull out of the pores (70). The frequency scan allows measurement of these properties in one scan so ensuring that tuning one property does not degrade another. This type of testing is not limited to adhesives as many materials see multiple frequencies in the actual use. Viscosity versus frequency plots are used extensively to study how changes in polymer structure or formulations affect the behavior of the melt. Often changes in materials, especially in uncured thermosetting resins and molten materials, affect a limited frequency range, and testing at a specific frequency can miss the problem.

It should be noted that since the material is scanned across a frequency range, there are some conditions where the material–instrument system acts like a guitar string and begins to resonate when certain frequencies are reached. These frequencies are either the natural resonance frequency of the sample–instrument system or one of its harmonics. This is shown in Figure 19. Under this set of experimental conditions, the sample–instrument system is oscillating like a guitar string and the desired information about the sample is obscured. Since there is no way to change this resonance behavior as it is a function of the system (in a free resonance analyzer, this effect is necessary), it is required

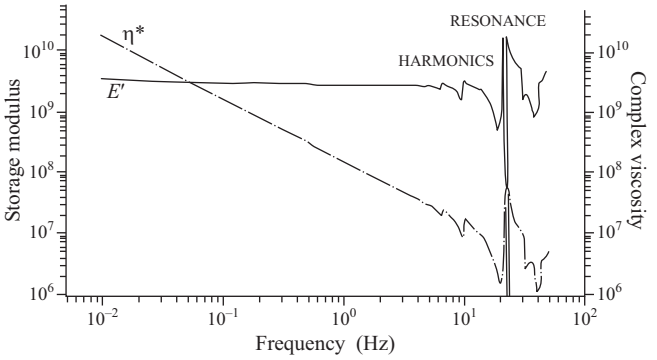

Fig. 19. Resonance effects.

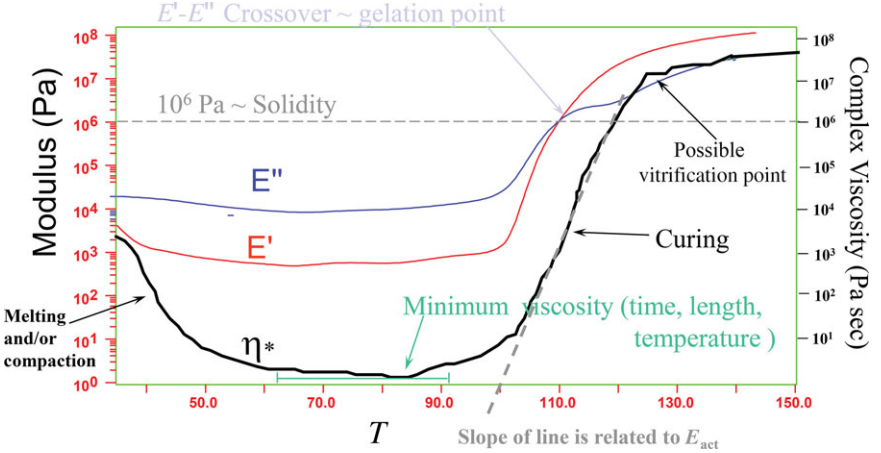

Fig. 20. Analysis of the cure profiles for a beta staged carbon fiber prepreg.

to redesign the experiment by changing sample dimensions or geometry to escape the problem. Often the design of the instrument will try and place the natural resonance frequency of the material outside its operating range (71). Even so, since it is changed by the sample, it does occur in real life. Using a sample with much different dimensions, which changes the mass, or changing from extension to three-point bending geometry changes the natural oscillation frequency of the sample and hopefully solves this problem.

4.3. Thermoset Curing. The DMA's ability to give viscosity and modulus values for each point in a temperature scan allow estimation of kinetic behavior as a function of viscosity. This has the advantage of describing how fluid the material is at any given time, so as to determine the best time to apply pressure, what design of tooling to use, and when the material can be removed from the mold. The simplest way to analyze a resin system is to run a plain temperature ramp from ambient to some elevated temperature (71). This "cure profile" allows collection of several vital pieces of information as shown in Figure 20.

4.3.1. Cure Studies in the DMA. Before analyzing the cure in Figure 20 in more detail, it should be mentioned that, in curing studies, all three types of commercial DMA's are used. The shape of curve and the temperature of events follow the same pattern. The values for viscosity and modulus often differ greatly. Both types of forced resonance DMA's also use samples impregnated into fabrics in techniques that are referred to as "torsional braid." There are some problems with this technique as temperature increases will cause an apparent curing of nondrying oils as thermal expansion increases friction. However, the "soaking of resin into a shoelace," as this technique has been called, allows one to handle difficult specimens under conditions where the pure resin is impossible to run in bulk (due to viscosity or evolved volatiles). Steel envelopes can also be used (73). Composite materials like graphite–epoxy composites are sometimes studied in industrial situations as the composite rather than the "neat" or pure resin because of the concern that the kinetics may be significantly different. In terms of ease of handling and sample, the composite is often easier to work with. Some axial instruments have addressed this with the development of specialized clamps for holding thin liquids in the shear mode. For example, the Mettler DMA/SDTA 861[e] low viscosity shear clamps can work with samples down to 2.5 Pa sec (approximately the viscosity of warm honey) when a very small gap is used.

Another special area of concern is paints and coatings (72) where the material is used in a thin layer. This can be addressed experimentally by either a braid as above or coating the material on a thin sheet of metal. The metal is often run first, and its scan is subtracted from the coated sheet's scan to leave only the scan of the coating. Envelopes of stainless steel sheet or fine mesh can also be used, and these containers also allow the running of powders and extremely fluid materials in an axial designed DMA (73). This is also done with thin films and adhesive coatings.

A sample cure profile for a commercial two-part epoxy resin is shown in Figure 20. From this scan, it is possible to determine the minimum viscosity ($\eta^*_{\min}$), the time to $\eta^*_{\min}$, and the length of time it stays there, the onset of cure, the point of gelation where the material changes from a viscous liquid to a viscoelastic solid, and the beginning of vitrification. The minimum viscosity is seen in the complex viscosity curve and is where the resin viscosity is the lowest. A given resin's minimum viscosity is determined by the resin's chemistry, the previous heat history of the resin, the rate at which the temperature is increased, and the amount for stress or stain applied. Increasing the rate of the temperature ramp is known to decrease the $\eta^*_{\min}$, the time to $\eta^*_{\min}$, and the gel time. The resin gets softer faster, but also cures faster. The degree of flow limits the type of mold design and when as well as how much pressure can be applied to the sample. The time spent at the minimum viscosity plateau is the result of a competitive relationship between the material's softening or melting as it heats and its rate of curing. At some point, the material begins curing faster than it softens, and that is where the viscosity starts to increase.

As the viscosity begins to climb, an inversion is seen of the E' and E'' values as the material becomes more solid-like. This crossover point also corresponds to where the tan δ equals 1 (since $E' = E''$ at the crossover). This is taken to be the gel

point (74), where the cross-links have progressed to forming an "infinitely" long network across the specimen. At this point, the sample will no longer dissolve in solvent. While the gel point correlates fairly often with this crossover, it does not always. For example, for low initiator levels in chain addition thermosets, the gel point precedes the modulus crossover (75). A temperature dependence for the presence of the crossover has also been reported (69). In some cases, where powder compact and melts before curing, there may be several crossovers (76). Then, the one following the $\eta^*_{\min}$ is usually the one of interest. Some researchers (77) believe the true gel point is best detected by measuring the frequency dependence of the crossover point. This is done by either by multiple runs at different frequencies or by multiplexing frequencies during the cure. At the gel point, the frequency dependence disappears (78). This value is usually only a few degrees different from the one obtained in a normal scan and in most cases not worth the additional time. During this rapid climb of viscosity in the cure, the slope for η^* increase can be used to calculate an estimated E_a (activation energy) (79). This will be discussed below, but the fact that the slope of the curve here is a function of E_a is important. Above the gel temperature, some workers estimate the molecular weight, M_c, between cross-links as:

$$G' = RT\rho/M_c \tag{28}$$

where R is the gas constant, T is the temperature in kelvins, and ρ is the density. At some point, the curve begins to level off and this is often taken as the vitrification point, T_{vf}.

The vitrification point is where the cure rate slows because the material has become so viscous that the bulk reaction has stopped. At this point, the rate of cure slows significantly. The apparent T_{vf} however is not always real: Any analyzer in the world has an upper force limit. When that force limit is reached, the "topping out" of the analyzer can pass as the T_{vf}. The use of a combined technique like DMA-DEA (80) to see the higher viscosities or the removal of a sample from parallel plate and sectioning it into a flexure beam is often necessary to see the true vitrification point. A reaction can also completely cure without vitrifying and will level off the same way. One should be aware that reaching vitrification or complete cure too quickly could be as bad as too slowly. Often a overly aggressive cure cycle will cause a weaker material as it does not allow for as much network development, but gives a series of hard (highly cross-linked) areas among softer (lightly cross-linked) areas.

On the way to vitrification, an important value is 10^6 Pa s. This is the viscosity of bitumen (81) and is often used as a rule of thumb for where a material is stiff enough to support its own weight. This is a rather arbitrary point, but is chosen to allow the removal of materials from a mold and the cure is then continued as a postcure step. As will be seen below, the postcure is often a vital part of the curing process.

The cure profile is both a good predictor of performance as well as a sensitive probe of processing conditions. A final note on cure profiles should be that a volume change occurs during the cure (82). This shrinkage of the resin is impor-

tant and can be studied by monitoring the probe position of some DMAs as well as by TMA and dilatometry.

4.3.2. Photocuring. A photocure in the DMA is run by applying a UV light source to a sample that is held a specific temperature or subjected to a specific thermal cycle (83). Photocuring is done for dental resin, contact adhesives, and contact lenses. UV exposure studies are also run on cured and thermoplastic samples by the same techniques as photocuring to study UV degradation. The cure profile of a photocure is very similar to that of a cake or epoxy cement. The same analysis is used and the same types of kinetics developed as is done for thermal curing studies.

The major practical difficulty in running photocures in the DMA is the current lack of a commercially available photocuring accessory, comparable to the photocalorimeters on the market. Several manufacturers now offer standard accessories to do UV curing in the DMA, and these attachments can often be adapted for Near Infrared (NIR) or Raman testing. The University of Colorado Dental School has adapted a DMA to allow simultaneous exposure to UV as well as monitoring by NIR (84), allowing the correlation of the chemical cure and mechanical properties.

4.3.3. Modeling Cure Cycles. The above discussions are based on using a simple temperature ramp to see how a material responds to heating. In actual use, many thermosets are actually cured using more complex cure cycles to optimize the trade-off between the processing time and the final product's properties (85). The use of two stage cure cycles is known to develop stronger laminates in the aerospace industry. Exceptionally thick laminates often also require multiple stage cycles to develop strength without porosity. As thermosets shrink on curing, careful development of a proper cure cycle to prevent or minimize internal voids is necessary.

One reason for the use of multistage cures is to drive reactions to completion. Another is to extend the minimum viscosity range to allow greater control in forming or shaping of the material. The development of a cure cycle with multiple ramps and holds would be very expensive if done with full sized parts in production facilities. The use of the DMA gives a faster and cheaper way of optimizing the cure cycle to generate the most efficient and tolerant processing conditions.

4.3.4. Isothermal Curing Studies. Often curing is done at a constant temperature for a period of time. This is how the data needed for the kinetic models discussed in the next section are normally collected. It is also how rubber samples are cross-linked, how initiated reactions are run, and how bulk polymerizations are performed. Industrially, continuous processes, as opposed to batch, often require an isothermal approach. UV light and other forms of nonthermal initiation also use isothermal studies for examining the cure at a constant temperature.

4.3.5. Curing Kinetics by DMA. Several approaches have been developed to studying the chemorheology of thermosetting systems. MacKay and Halley (86) recently reviewed chemorheology and the more common kinetic models. A funda-

mental method is the Williams–Landel–Ferry model (87), which looks at the variation of T_g with degree of cure. This has been used and modified extensively (88). A common empirical model for curing has been proposed by Roller (89). In the latter approach, samples of the thermoset are run isothermally as described above and the viscosity versus time data collected. This is plotted as log η^* versus time in seconds, where a change in slope is apparent in the curve. This break in the data indicates the sample is approaching the gel time. From these curves, the initial viscosity, η_0, and the apparent kinetic factor, k, can be determined. By plotting the log viscosity versus time for each isothermal run, the slope, k, and the viscosity at $t = 0$ are apparent. The initial viscosity and k can be expressed as

$$\eta_o = \eta_\infty e^{\Delta E_\eta/RT} \tag{29}$$

$$k = k_\infty e^{\Delta E_k/RT} \tag{30}$$

Combining these allows to set up of the equation for viscosity under isothermal conditions as

$$\ln \eta(t) = \ln \eta_\infty + \Delta E_\eta/RT + tk_\infty e^{\Delta E_k/RT} \tag{31}$$

By replacing the last term with an expression that treats temperature as a function of time, the equation becomes

$$\ln \eta(T, t) = \ln \eta_\infty + \Delta E_\eta/RT + \int_0^t k_\infty e^{\Delta E_k/RT} dt \tag{32}$$

This equation can be used to describe viscosity–time profiles for any run where the temperature can be expressed as a function of time. The activation energies can now be calculated. The plots of the natural log of the initial viscosity (determined above) versus $1/T$ and the natural log of the apparent rate constant, k, versus $1/T$ are used to give us the activation energies, ΔE_η and ΔE_k. Comparison of these values to the k and ΔE to those calculated by DSC shows that this model gives larger values (70). The DSC data are faster to obtain, but they do not include the needed viscosity information.

Several corrections have been proposed, addressing different orders of reaction (90) (the above assumes first order) and modifications to the equations (92). Many of these adjustments are reported in Roller's 1986 review (92) of curing kinetics. It is noted that these equations do not work well above the gel temperature. This same equation has been used to predict the degradation of properties in thermoplastics successfully (93).

4.3.6. Mapping Thermoset Behavior: The Gillham–Enns Diagram. Another approach to attempt to fully understand the behavior of a thermoset was developed by Gillham and co-workers (94) and is analogous to the phase diagrams used by metallurgists. The time–temperature–transformation diagram (TTT) or the Gillham–Enns diagram (after its creators) is used to track the effects of temperature and time on the physical state of a thermosetting material.

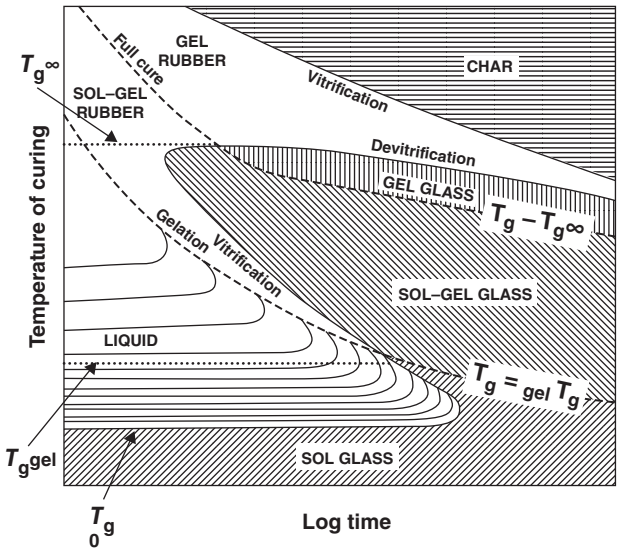

Fig. 21. Gillham–Enns diagram.

Figure 21 shows an example. Running isothermal studies of a resin at various temperatures and recording the changes as a function of time can do this. One has to choose values for the various regions, and Gillham has done an excellent job of detailing how one picks the T_g, the glass, the gel, the rubbery, and the charring regions (95). These diagrams are also generated from DSC data (96), and several variants (97), such as the continuous heating transformation and conversion–temperature–property diagrams, have been reported. Surprisingly easy to do, although a bit slow, they have not yet been accepted in industry despite their obvious utility. A recent review (98) will hopefully increase the use of this approach.

Symbols, Abbreviations, and Acronyms

E_a	Activation energy
E^*	Complex Modulus
E'	Storage Modulus
E''	Loss Modulus
f	Frequency
G	Shear modulus
J	Compliance
k	Deformation
k	Rate constant
M_e	Entanglement molecular weight
M_c	Molecular weight between cross-links
M_w	Molecular weight
T	Period

$T_{\alpha,\beta,\gamma}$	Transition (subscript type)
v^{f}	Free volume
Λ	Logarithmic decrement
γ	Shear strain
$\dot{\gamma}$	Shear strain rate
δ	Phase angle
$\tan\delta$	Tangent of the phase angle, also called the damping
ε	Tensile strains
$\dot{\varepsilon}$	Strain rate
η	Viscosity
η^*	Complex viscosity
η'	Storage viscosity
η''	Loss viscosity
Γ	Torque
ρ	Density
σ	Stress
ω	Frequency, Hz
DEA	Dielectric analysis or analyzer
DSC	Differential scanning calorimeter
DMA	Dynamical mechanical analysis or analyzer
DMTA	Dynamic mechanical thermal analysis or analyzer
TBA	Torsional braid analyzer
TGA	Thermogravimetric analyzer

Acknowledgments

The authors wish to acknowledge the help and support of Mettler-Toledo NA, especially B. Weddle, and the Laboratory for Advanced Materials and Optimized Processing at the University of North Texas, especially Prof. W. Brostow.

BIBLIOGRAPHY

1. N. McCrum, B. Williams, and G. Read, *Anelastic and Dielectric Properties of Polymeric Solids*, Dover Publications, N. Y., 1991, pp. 192–200.
2. (a) K. Menard, *Dynamic Mechanical Analysis: A Practical Introduction*, CRC Press, Boca R aton, Fla., 1999; (b) M. Sepe, *Dynamic Mechanical Analysis for Plastic Engineering*, Plastic Design Library, New York, 1998; (c) T. Murayama, *Dynamic Mechanical Analysis of Polymeric Materials*, Elsevier Science Publishing Co., New York, 1977.
3. J. H. Poyntang, *Proc. R. Soc., Series A* **82**, 546 (1909).
4. A. Kimball and D. Lovell, *Trans. Am. Soc. Mech. Eng.* **48**, 479 (1926).
5. K. te Nijenhuis, in G. Astarita, G. Marruci, and L. Nicolais, ed., *Rheology Volume 1: Principles*. Plenum Press, New York, 1980, pp. 263.
6. M. L. Miller, *The Structure of Polymers*, Reinhold Publishing, New York, 1966.
7. J. Dealy, *Rheometers for Molten Plastics*, Van Nostrand Reinhold, New York, 1992, pp. 136–137 and 234–236.
8. J. Ferry, *Viscoelastic Properties of Polymers*, 3rd ed., John Wiley & Sons, New York, 1980.

9. N. McCrum, B. Williams, and G. Read, *Anelastic and Dielectric Effects in Polymeric Solids*, Dover Publications , New York, 1991.
10. J. Gilham and J. Enns, *Trends Polym. Sci.* **2**, 406 (1994).
11. C. Macosko and J. Starita, *SPE J.* **27**, 38 (1971).
12. T. Murayama, *Dynamic Mechanical Analysis of Polymeric Materials*, Elsevier Science Publishing Co., New York, 1977.
13. B. E. Read and G. D. Brown, *The Determination of the Dynamic Properties of Polymers and Composites*, John Wiley & Sons, New York, 1978.
14. American Standards and Test Methods: http://www.astm.org/
15. (a) J. Gillham, in J. Dworkins, ed., *Developments in Polymer Characterizations: Volume 3*, Applied Science Publisher, Princeton, N.J., 1982, pp. 159–227; (b) J. Gillham and J. Enns, *Trends Polym. Sci.* **2**(12), 406 (1994).
16. U. Zolzer and H-F. Eicke, *Rheol. Acta* **32**, 104, (1993).
17. N. McCrum, B. Williams, and G. Read, *Anelastic and Dielectric Properties of Polymeric Solids*, Dover Publications, New York, 1991, pp. 192–200.
18. P. Flory, *Principles of Polymer Chemistry*, Cornell University Press, I thaca, N.Y., 1953.
19. R. Bird, C. Curtis, R. Armstrong, and O. Hassenger, *Dynamics of Polymer Fluids*, 2nd ed., John Wiley & Sons, New York, 1987.
20. (a) J. D. Ferry, in Ref. 8; (b) J. J. Aklonis and W. J. McKnight, *Introduction to Polymer Viscoelasticity*, 2nd ed., John Wiley & Sons, New York, 1983.
21. (a) L. C. E. Struik, *Physical Aging in Amorphous Polymers and Other Materials*, Elsevier Science Publishing Co., New York, 1978; (b) L. C. E. Struik, in W. Brostow and R. D. Corneliussen, eds., *Failure of Plastics*, Hanser Publications, New York, 1986; (c) S. Matsuoka, in W. Brostow and R. D. Corneliussen, eds. *Failure of Plastics*, Hanser Publications, New York, 1986; (d) S. Matsuoka, *Relaxation Phenomena in Polymers*, Hanser Publications, New York, 1992.
22. J. D. Vrentas, J. L. Duda, and J. W. Huang, *Macromolecules* **19**, 1718 (1986).
23. W. Brostow and M. A. Macip, *Macromolecules* **22**(6), 2761 (1989).
24. N. McCrum, G. Williams, and B. Read, *Anelastic and Dielectric Effects in Polymeric Solids*, Dover Publications , New York, 1967.
25. M. Doi and S. Edwards, *The Dynamics of Polymer Chains*, Oxford University Press, New York, 1986.
26. A. Aklonis and J. Knight, *Introduction to Viscoelasticity*, John Wiley & Sons, New York, 1983.
27. C. L. Rohn, *Analytical Polymer Rheology*, Hanser-Gardener Publications, New York, 1995.
28. J. Heijboer, *Int. J. Polym. Mater.* **6**, 11 (1977).
29. N. McCrum, G. Williams, and B. Read, *Anelastic and Dielectric Effects in Polymeric Solids*, Dover Publications, New York, 1967.
30. R. F. Boyer, *Polym. Eng. Sci.* **8** (3), 161 (1968).
31. C. L. Rohn, in Ref. 21, pp. 279–283.
32. (a) J. Heijboer, *Int. J. Polym. Mater.* **6**, 11 (1977); (b) M. Mangion and G. Johari, *J. Polym. Sci, Part B: Polym. Phys.* **29**, 437 (1991); (c) G. Johari, G. Mikoljaczak, and J. Cavaille, *Polymer* **28**, 2023 (1987); (d) S. Cheng et al., *Polym. Sci. Eng.* **33**, 21 (1993); (e) G. Johari, *Lect. Notes Phys.* **277**, 90 (1987); (f) R. Daiz-Calleja and E. Riande, *Rheol. Acta* **34**, 58 (1995); (g) R. Boyd, *Polymer* **26**, 323 (1985); (h) V. Bershtien, V. Egorov, L. Egorova, and V. Ryzhov, *Thermochim. Acta* **238**, 41 (1994).
33. B. Twombly, *Proc. NATAS* **20**, 63 (1991).
34. (a) C. L. Rohn, *Analytical Polymer Rheology*, Hanser: Cincinnati, (1995), 185–210; (b) J. Heijboer, *Int. J. Polym. Mater.* **6**, 11 (1977).
35. R. Boyer, *Polym. Eng. Sci.* **8**(3), 161 (1968).

36. V. Bershtien and V. Egorov, *Differential Scanning Calorimetery in the Physical Chemistry of Polymers*, Ellis Horwood, Chich ester, UK, 1993.
37. B. Coxton, personal communication , 1998.
38. S. Cheng et al., *Polym. Sci. Eng.* **33**, 21 (1993).
39. G. Johari, G. Mikoljaczak, and J. Cavaille, *Polymer* **28**, 2023 (1987).
40. M. Mangion and G. Johari, *J. Polym. Sci, Part B: Polym. Phys.* **29**, 437 (1991).
41. (a) F. C. Nelson, *Shock Vib. Dig.* **26**, 11 (1994); (b) F. C. Nelson, *Shock Vib. Dig.* **26**, 24 (1994).
42. W. Brostow, personal communication, 2004.
43. R. Boyer, *Polym. Eng. Sci.* **8**(3), 161 (1968).
44. (a) G. Johari, *Lect. Notes Phys.* **277**, 90 (1987); (b) J. Heijboer, *Int. J. Polym. Mater*. **6**, 11 (1977); (c) J. Heijboer, in J. Prins, ed., *Physics of Non-Crystalline Solids*, Interscience, New York, 1965; (d) J. Heijboer, *J. Polym. Sci.* **C 16**, 3755 (1968); (e) L. Nielsen, *J. Macromol. Sci., Phys.* **9**, 239 (1974).
45. A. Yee and S. Smith, *Macromolecules* **14**, 54 (1981).
46. G. Gordon, *J. Polym. Sci. A2* **9**, 1693 (1984).
47. J. Wendorff and B. Schartel, *Polymer* **36**, 899 (1995).
48. R. H. Boyd, *Polymer* **26**, 323 (1985).
49. (a) I. Noda, *Appl. Spectrosc.* **44**(4), 550 (1990); (b) V. Kien, *Proc. 6th Sympos. Radiat. Chem.* **6**, 463 (1987).
50. L. H. Sperling, *Introduction to Physical Polymer Science*, 2nd ed., John Wiley & Sons, New York, 1992.
51. C. Macosko, *Rheology*, VCH Publishers, New York, 1994.
52. (a) F. Quinn and T. Hatakeyama, *Thermal Analysis*, John Wiley & Sons, New York, 1994; (b) B. Wunderlich, *Thermal Analysis*, Academic Press, New York, 1990.
53. (a) J. Schawe, *Thermochim. Acta* **261**, 183 (1995); (b) J. Schawe, *Thermochim. Acta* **260**, 1 (1995); (c) J. Schawe, *Thermochim. Acta* **271**, 1 (1995); (d) B. Wunderlich, A. Boller, and Y. Yin, *J. Therm. Anal.* **42**, 949 (1994); (e) P. Cortes, I. Fraga, Y. Calventus, F. Roman, J. Hutchinson, and F. Ferrando. *Materials* **7**, 1830–1849 (2014); (f) A. Hammer, ed., *Applications of Thermal Analysis,* Mettler Toledo Inc., Greifensee, Switzerland, 2012, pp. 12–14.
54. (a) R. H. Boyd, *Polymer* **26**, 323 (1985); (b) R. H. Boyd, *Polymer* **26**, 1123 (1985).
55. (a) S. Godber, personal communication, 2001; (b) M. Ahmed, *Polypropylene Fiber- Science and Technology*, Elsevier Science, New York, 1982.
56. A. Lobanov and S. Frenkel, *Polym. Sci. USSR* **22**, 1150 (1980).
57. (a) R. Boyer, *J. Polym Sci., Part B: Polym. Phys.* **30**, 1177 (1992); (b) J. K. Gilham et al., *J. Appl. Polym. Sci.* **20**, 1245 (1976); (c) J. B. Enns and R. Boyer, *Encycl. Polym. Sci.* **17**, 23–47 (1989).
58. V. Bershtien, V. Egorov, L. Egorova, and V. Ryzhov, *Thermochim. Acta.* **238**, 41 (1994).
59. C. M. Warner, MS thesis, Central Michigan State University, 1988.
60. (a) B. Cassel, PETAN #69 DDSC, Perkin-Elmer, Norw alk, Conn., 1995; (b) W. Sichina, *Proc. NATAS* **23**, 137 (1994); (c) B. Wunderlich, A. Boller, and Y. Jin, *J. Therm. Anal* 1994, **42**, 307 (1994); (d) B. Wunderlich, *Modulated DSC*, Univesity of Tennessee., Knoxvil le, Tenn., 1994.
61. (a) J. Dealy, *Melt Rheology and its Role in Plastic Processing*, Van Nostrand Reinhold, Toronto, Canada, 1990; (b) N. Chereminsinoff, *An Introduction to Polymer Rheology and Processing*, CRC Press, Boca Rat on, Fla., 1993.
62. (a) E. Turi, ed., *Thermal Characterization of Polymeric Materials*, Academic Press, Bosto n, Mass., 1981; (b) E. Turi, ed., *Thermal Analysis in Polymer Characterization*, Heydon, London, 1981.
63. C. Rohn, in Analytical Polymer Rheology, Hanser: Cincinnati, (1995), p. 203.
64. M. Miller, *The Structure of Polymers*, Reinhold, New York, 1966, pp. 611–612.

65. S. Rosen, *Fundamantal Principles of Polymeric Materials*, Wiley Interscience, New York, 1993, pp. 53–77 and 258–259.
66. (a) W. Cox and E. Merz, *J. Polym. Sci.* **28**, 619 (1958); (b) P. Leblans, H. Booj, J. Palmer, and G. Tiemersma-Thone, *J. Polym. Sci.* **21**, 1703 (1983).
67. W. Gleissele, in G. Astarita, G. Marruci, and L. Nicolais, eds., *Rheology, Volume 2*, Plenum Press, New York, 1980, pp. 457.
68. D. W. Van Krevelin, *Properties of Polymers*, Elsevier Science, New York, 1987, p. 289.
69. C. Macosko, *Rheology*, VCH Publishers, New York, 1996, pp. 120–127.
70. (a) L.-H. Lee, ed., *Adhesive Bonding*, Plenum Press, New York, 1991; (b) L.-H. Lee, ed., *Fundamentals of Adhesion*, Plenum Press, New York, 1991.
71. (a) G. Martin, A. Tungare, and J. Gotro, *Polymer Characterization*, ACS, Washington D. C., 1990; (b) M. Ryan, *ANTEC Proc.* **31**, 187 (1973); (c) C. Gramelt, *Am. Lab.* January, 26 (1984); (d) S. Etoh, *SAMPE J.* **3**, 6 (1985); (f) F. Hurwitz, *Polym. Compos.* **4**(2), 89 (1983).
72. (a) M. Roller, *Polym. Eng. Sci.* **19**, 692 (1979); (b) M. Roller, and J. Gilham, *J. Coating Technol.* **50**, 57 (1978).
73. (a) F. Warren, P. Royall, P. Butterworth, and P. Ellis, *Carbohydrate Polymers* **90**, 628 (2012); (b) P. Royall, C. Huang, S. Tang, J. Duncan, and M. Brown, *Int. J. Pharm* **301**, 181 (2005); (c) R. Ou, Y. Xie, Q. Wang, S. Sui, and M. Wolcott, *Holzforschung* **69**, 223 (2015).
74. (a) M. Heise, *Polym. Eng. Sci.* **30**, 83 (1990); (b) K. O'Driscoll, *J. Polym. Sci.: Polym. Chem.* **17**, 1891 (1979); (c) O. Okay, *Polymer* **35**, 2613 (1994).
75. M. Hiese and G, Martin, *J. Gotro, Polymer Eng. Sci.* **30** (2), 83 (1990).
76. K. Wissbrun, D. Rhun, and M. Hannon, *J. Coating Technol.* **48**, 42 (1976).
77. (a) F. Champon, *J. Rheol.* **31**, 683 (1987); (b) H. Winter, *Polym. Eng. Sci.* **27**, 1698 (1987); (c) C. Michon, G. Culvelier, and B. Launay, *Rheol. Acta* **32**, 94 (1993).
78. C. Michon, G. Culvelier, and B. Launay, *Rheol. Acta* **32**, 94 (1993).
79. I. Kalnin and K. Hollands, *Epoxy Resins*, ACS, Washington D.C., 1970.
80. DEA is dielectric analysis, where an oscillating electrical signal is applied to a sample. From this signal, the ion mobility can be calculated, which is then converted to a viscosity (see McCrum for details). DEA will measure to significantly higher viscosities than DMA.
81. H. Barnes, J. Hutton, and K. Walters, *An Introduction to Rheology*, Elsevier Science Publishing, Co., New York, 1989.
82. A. W. Snow, and J. Armistead, *J. Appl. Polym. Sci.* **52**, 401, 1994.
83. (a) T. Renault, *NATAS Notes* **25**, 44 (1994); (b) H. L. Xuan and C. Decker, *J. Polym. Sci.: Part A* **31**, 769 (1993); (c) W. Shi and B. Ranby, *J. Appl. Polym. Sci.* **51**, 1129 (1994).
84. (a) J. Stansbury, H. Lu, J. Nie, and C. Bowman, *Dental Mater.* **25**, 33–38 (2009); (b) C. Bowman, H. Kilambi, H. Lu, P. Shah, and J. Stansbury, *Biomaterials* **26**, 1329–1336 (2005).
85. (a) R. Geimer, R. Follens, J. Kowtsky, A. Christensen, and G. Myers, *J. Appl. Polym. Sci.* **47**, 1481 (1993); (b) R. Roberts, *SAMPE J.* **5**, 28 (1987).
86. P. J. Halley and M. E. MacKay, *Polym. Eng. Sci.* **36**(5), 593 (1996).
87. J. Ferry, Viscoelastic Properties of Polymer, Wiley and Sons: New York, (1980) 266–330.
88. (a) J. Mijovic, *J. Comp. Met.* **23**, 163 (1989); (b) J. Mijovic, *SAMPE J*. **23**, 51 (1990).
89. (a) M. Roller, *Metal Finishing* **78**, 28 (1980); (b) M. Roller, *ANTEC Proc.* **24**, 9 (1978); (c) J. Gilham, *ACS Symp. Series* **78**, 53 (1978); (d) M. Roller, *ANTEC Proc*. **21**, 212 (1975); (e) M. Roller, *Polym. Eng. Sci.* **15**, 406 (1975); (f) M. Roller, *Polym. Eng. Sci.* **26**, 432 (1986).
90. C. Rohn, *Problem Solving for Thermosetting Plastics*, Rheometrics, Austin, Tex., 1989.

91. (a) J. Seferis, M. Dusi, and C. May, *Chemorheology of Thermosetting Polymers*, ACS, Washington, D.C. 1983, pp., 301; (b) R. Patel and S. Patel, *J. Therm. Anal.* **39**, 229 (1993).
92. M. Roller, *Polym. Eng. Sci.* **26**, 432 (1986).
93. M. Roller, personal communication 1998.
94. (a) J. Gillham and N. Schneider, *Polym. Compos.* **1**, 97 (1980); (b) J. Enns, and J. Gilham, *J. Appl. Polym. Sci.* **28**, 2567 (1983); (c) L. C. Chan, N. Noe, and J. Gilham, *J. Appl. Polym. Sci.* **29**, 3307 (1984); (d) J. Gillham, *Polym. Eng. Sci.* **26**, 1429 (1986); (e) S. Simon, J. Gilham, *J. Appl. Polym. Sci.* **51**, 1741 (1994); (f) G. Palmese, J. Gilham, *J. Appl. Polym. Sci.* **34**, 1925 (1987); (g) J. Enns, and J. Gilham, in C. Craver, ed., *Polymer Characterization*, ACS, Washington, D.C., 1983.
95. (a) J. Gillham and S. Simon, *J. Appl. Polym. Sci.* **53**, 709 (1994); (b) J. Enns and J. Gillham, *Trends Polym. Sci.* **2**, 406 (1994).
96. A. Otero, M. Clavaguera-Mora, S. Surinach, M. Baro, and N. Clavaguera, *Thermochim. Acta* **203**, 379 (1992).
97. (a) J. Gillham and G. Wisenrakkit, *J. Appl. Polym. Sci.* **42**, 2453 (1991); (b) B. Osinski, *Polymers* **34**, 752 (1993).
98. J. Enns and J. Gillham, *Trends Polym. Sci*. **2**, 406 (1994).

KEVIN P. MENARD
Mettler Toledo, Columbus, OH, USA

NOAH R. MENARD
Veritas Testing and Consulting LLC, Denton, TX, USA